Photonics West
Micromachinig and Microfabrication
25-31 January 2003, San Jose, California, USA
Conference on MOEMS and Miniaturized Systems III (mf05)

THIN FILM TECHNOLOGY BASED MICRO-FOURIER SPECTROMETER

D. Knipp[a,b*], H. Stiebig[b], S.R. Bhalotra[c], H.L. Kung[c], D.A.B. Miller[c]

a) IMEC, Advanced Components and Sensor Systems, 3001 Leuven, Belgium
b) Research Center Jülich, Institute of Photovoltaic, 52425 Jülich, Germany
c) Stanford University, Ginzton Laboratory, Stanford, CA 94305

ABSTRACT

A novel Fourier spectrometer using thin film technology was developed. The spectrometer based on a semi transparent thin film detector in combination with a tunable micro machined mirror. The semi transparent detector is introduced into a standing wave created in front of the mirror to sample the profile of the standing wave. Varying the position of the mirror results in a shift of the phase of the standing waves and thus in a change of the optical generation profile within the semi transparent detector. The active region of the sensor (thickness · absorption) is thinner than the wavelength of the incoming light, so that the modulation of the intensity results in a modulation of the overall photocurrent. The spectral information of the incoming light can be determined by the Fourier transformation of the sensor signal. Based on the linear arrangement of the sensor and the mirror, the spectrometer facilitates the realization of 1D and 2D arrays of spectrometers combining medium range spectral resolution with medium range spatial resolution. The novel device is filling the gap between solid-state camera technology with only three-color channels (red, green and blue) but high spatial resolution on one hand and precision spectrometers with high spectral resolution but no spatial resolution on the other hand. An analytical optical model of the spectrometer was applied to evaluate different detector concepts. The model was used to study the performance of different device designs regarding the spectral resolution of the spectrometer, the spectral range and the linearity of the response. The calculations will be compared with experimental results of semi transparent amorphous silicon detectors.

Keywords: Fourier Spectrometer, Spectrometer, thin films, optical sensor, multispectral imaging, MEMS

1. INTRODUCTION

Various miniature interferometers and spectrometers for different applications have been developed in recent years [1-3]. Especially the interest in optical MEMS technology has initiated a lot of new research activities in optical metrology. The activities are driven by improvements of size, cost and performance. Consequently, several interferometers and spectrometer concepts have been transferred from the macro to the micro scale like Michelson Interferometers, Fabry-Perot interferometers/spectrometers [1], grating spectrometers [2] and Fourier spectrometers [3].

Most of the interferometers/spectrometer concepts are limited by the fact that 1D and 2D spectrometer arrays cannot be realized or the realization requires high technological effort. Nevertheless 1D and 2D spectrometer arrays are of interest in the area of multispectral imaging or hyperspectral imaging. Multispectral imaging systems are frequently used in life science, military, surveillance and inspection in general [4].

In the following paper we will present a new concept of a spectrometer for the visible part of the spectrum. The concept of the spectrometer based on the sampling of a standing wave by a semi transparent optical detector. Using the effect of a standing wave to realize wavelength sensitive detectors [5], interferometers and

* Correspondance: Email: knipp@imec.be, WWW:http://www.imec.be; phone: ++32 16 28 1062; Fax: ++32 16 28 1501.

spectrometers is known for many years [6-8], but the realization of such a concept has been limited by technological reasons. Sampling of a standing wave by a semiconductor device requires a highly transparent and very thin detector. Otherwise no light is transmitted through the sensor and no standing wave is created. On the other hand sufficient light has to be absorbed to generate an electrical signal as a consequence of the modulation of the optical generation profile within the sensor. The active region of the sensor should be thinner than the wavelength of the incoming light so that the overall photocurrent is modulated as a function of the position of the mirror. Using silicon-based detectors to realize spectrometers in the visible part of the spectrum requires a thickness of the active region of 30-50nm [5]. In the case of a thicker active layer the photocurrent is still modulated but the amplitude of the modulated signal is reduced. However, the sensor can consist of additional layers, which are not photoelectrical active but provide additional functionality like transparent contact layers or anti reflection coatings.

Kung and Bhalotra [8] have presented the first Fourier spectrometer utilizing the effect of sampling a standing wave for spectrometer applications. In the case of Kung a thin amorphous silicon coplanar photoconductor structure was applied to sample a standing wave created in front of a micro-machined mirror. The novel spectrometer reduces the number of components to a minimum, simplifies the setup to a linear arrangement of a detector and a mirror and facilitates the realization of 1D or 2D spectrometer arrays.

The performance of the spectrometer is mainly determined by the accuracy of the thin film processing, the optoelectronic properties of the active thin films, the interaction of the standing wave with the detector and the performance of the MEMS based mirror. In this paper we will mainly discuss the interaction between the semi transparent detector and the standing wave. In section 2 and 3, we will give a detailed description of the optics in such a spectrometer. Furthermore, we will discuss different detector designs (section 4). The calculations will be compared with experimental results in section 5, before discussing the implications of different sensor designs in section 6.

2. FUNDAMENTALS

2.1 Standing Wave

The interference of two waves can be described by the superposition of two waves propagating into the same or opposite directions. The amplitude and the phase of the electric field determine the intensity at each spatial position of the interference pattern. The intensity of the superposition of the two waves can be described by

$$I_S(x) = I_1(x) + I_2(x) + 2 \cdot \sqrt{I_1(x) I_2(x)} \cos\left(\frac{4\pi \cdot d_m}{\lambda}\right) \tag{1}$$

$I_1(x)$ and $I_2(x)$ are the intensities and $4\pi \cdot d_m/\lambda$ is the phase difference of the two light beams. In the case of a Michelson Interferometer the standing wave in the detector arm is created by the superposition of two waves propagating into the same direction and d_m corresponds to the relative difference of the reference and measuring mirror. We can assume the intensity of the two beams to be equal, $I_1(x)= I_2(x)=I_0$, so that equation 1 is simplified to

$$I_S = 2I_0\left(1+\cos\left(\frac{4\pi \cdot d_m}{\lambda}\right)\right) = 4I_0 \cos^2\left(\frac{2\pi \cdot d_m}{\lambda}\right) \tag{2}$$

As a consequence the signal modulates between 0 (destructive interference) and $4 \cdot I_0$ (constructive interference).

2.2 Standing Wave Interferometer/spectrometer

In the case of a standing wave spectrometer the two waves, which were superimposed, propagate into opposite directions. The working principle of the spectrometer is schematically depicted in figure 1. Figure 1 exhibits the ideal case of a standing wave spectrometer. The reflection of the incoming intensity I_0 leads to the creation of the

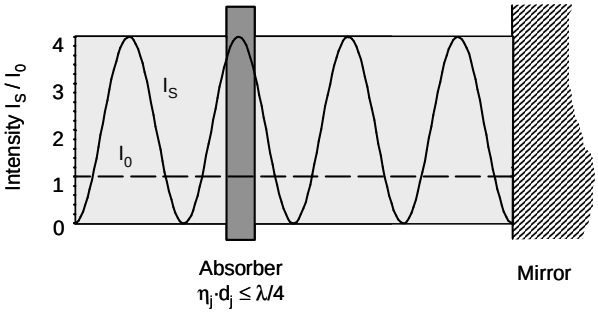

Fig. 1: Schematic setup of a standing wave spectrometer consisting of a semi transparent optoelectrical active absorber and a mirror.

standing wave in front of the mirror. By modulating the detector or the reflector, the optical generation profile within the detector changes between 0 and $4 \cdot I_0$. The wavelength of the standing wave corresponds to half of the wavelength of the incoming light. Due to the absorption of a fraction of the incoming light the reflected light intensity is always smaller than the incoming light intensity ($I_1(x) > I_2(x)$). Therefore, the ideal case of a complete constructive or destructive interference is usually not reached (figure 1 depicts the ideal case of a complete destructive and constructive interference). The difference between $I_1(x)$ and $I_2(x)$ results in a constant photocurrent, which is superimposed to the photocurrent modulated by the position of the mirror.

Schematic sketches of standing wave spectrometers are shown in figure 2. A coplanar photoconductor structure on a glass substrate is used as a semi transparent sensor in figure 2a. The photo-generation of carriers results in a change of the photoconductivity of the thin film. The current flow is perpendicular to the standing wave. The processing of such a structure is relative simple, because metal electrodes can be used to form the contacts. A sandwich structure is shown in figure 2b, which can be applied as a semi transparent sensor. The electrodes were formed by transparent conductive oxide layer like ITO (indium tin oxide), ZnO or SnO_2. In this case the photocurrent flow is parallel to the standing wave. The implications of the different device designs and their impact on the device performance will be discussed in the following.

3. OPTICAL MODEL

In order to describe the wave propagation within the semi transparent sensor, we have developed a one-dimensional analytical optical model according to the Airy formalism [8]. We applied matrix formalism to calculate the electric field, the optical generation and the reflection of the multi-layer structure. Based on the matrix formalism the performance of the spectrometer can be described by a linear function, which directly correlates the input and the output electric field vector. The details of the optical model are described elsewhere [9,10]. The formalism is applied to the multi-layer system shown in Fig. 3. Figure 3 exhibits a universal layer structure, which consists of a semi transmissive detector, an air gap and a mirror. The component $E_{0,1}^{+}$ describes

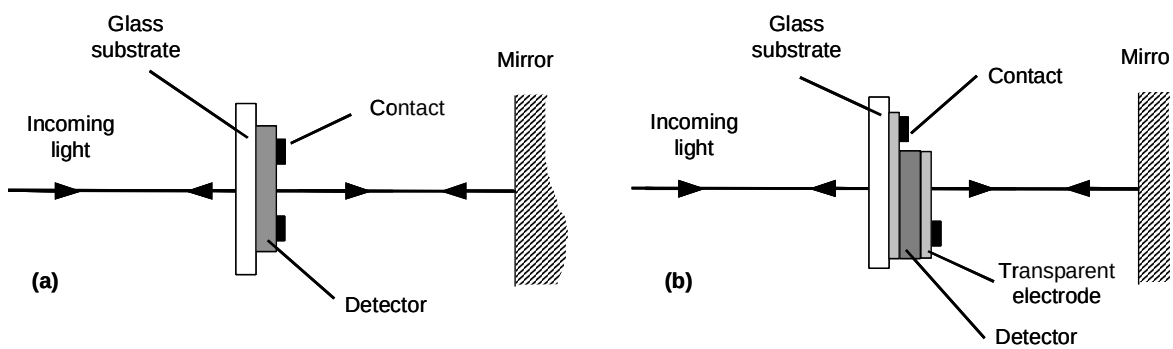

Fig. 2: Schematic sketch of Fourier spectrometers based on sampling a standing wave. Light reflected by the mirror creates a standing wave in front of the mirror, which is detected by the semi transparent detector. The semi transparent sensor can be formed by a coplanar photoconductor (a) or a sandwich structure (b).

the electric field towards the first interface within positive direction, whereas $E_{0,1}^{-}$ represents the electric field at the interface between layer 0 and 1 in negative directions. Hence, the components $E_{m+1,m}^{+}$ indicate the electric output field at the interface between the m- and m+1-layer. The layer m+1 represents the mirror, so that $E_{m+1,m}^{-}$ becomes zero. In this case the layer j represents the optoelectronic active layer of the detector and the layer m corresponds to the air gap between the detector and the mirror. In order to simplify the description of the optical wave propagation, the layer stack can be divided into a four-layer system based on the j-layer (active region of the sensor), the two subsystems S_1 (layer 1 to j-1) and S_2 (layer j+1 to m-1) and the m-layer (air gap between the mirror and the detector). At this point we assume that the mirror has a reflectivity of 100%. Therefore, the transmission and the reflection of the system can be defined. Based on this expression the electric field in the j-layer can be calculated as a superposition of the electric field into positive and negative directions. Afterwards the intensity within the layer j can be calculated after a few transformations [9, 10].

$$I_j(x,d_m,\lambda)=I_0T_0(\lambda)\frac{\eta_j}{\eta_0}\left(e^{-\alpha_j x}+(\tau_2)^2\cdot e^{-\alpha_j(2d_j-x)}-2\cdot\tau_2\cdot e^{-\alpha_j d_j}\cdot\cos\left(\frac{4\pi}{\lambda}\left[\eta_j(d_j-x)+\eta_m d_m\right]+2\xi_2\right)\right) \quad (3)$$

I_0 is the incident light intensity and $T_0(\lambda)$ corresponds to an internal transmission of the multi-layer system. α_j is the absorption coefficient of the j-layer ($\alpha_j=4\pi\kappa_j/\lambda$). η_j, η_0 are the real components of the complex refractive indexes of the j-layer and the ambient layer (typically air). τ_2 and ξ_2 are the absolute value and the phase of the transmission of the subsystem S_2. The first term $\exp(-\alpha_j x)$ of equation 3 originates from the electric field propagation into positive direction. The positive direction means the direction of the incident light. The second term $\exp(-\alpha_j(d_j-x))$ describes the electric field propagation into negative direction. The third term is due to interference effects of the two waves.

In order to study the behavior of the spectrometer we determined the sensitivity (SEN), the differential sensitivity (SD) and the standing wave effect (SWE). First we calculated the sensitivity (SEN) by an integration of the intensity over the active layer (j-layer). For simplicity we assumed that the transmission of the layer stack S_2 is equal to 1 ($\tau_2=1$) and the phase information of the subsystem S_2 is equal to 0 ($\xi_2=0$). In the first step we neglected the effect of interference on the sensitivity. After the integration the sensitivity results to

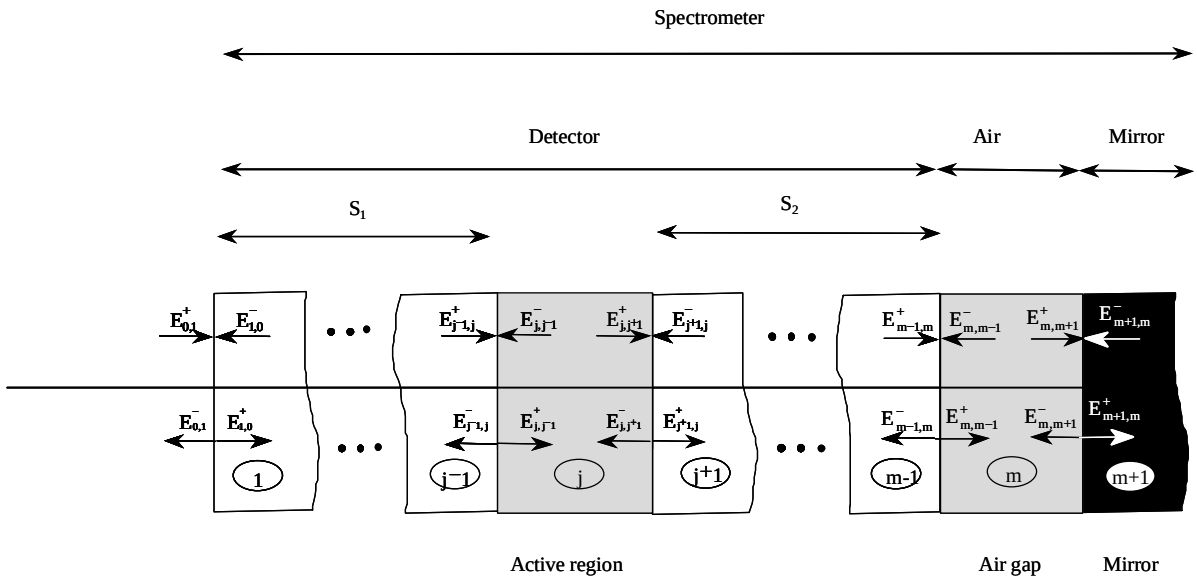

Fig. 3: Schematic sketch of a spectrometer based on a multi layer system. The layer j represents the optoelectronic active layer of the detector and the layer m corresponds to the air gap between the mirror and the detector. The system consists of the subsystem S_1, the optoelectronic active layer j, the subsystem S_2, the air gap layer m and the mirror (layer m+1).

$$SEN(\lambda) = I_0 \frac{\eta_j}{\eta_0} \int_0^{d_j} \left(\exp(-\alpha_j x) + \exp(-\alpha_j (2d_j - x))\right) dx = \frac{k_0}{\alpha_j} \left(1 - \exp(-2\alpha_j d_j)\right) \tag{4}$$

The constant k_0 is equal to $I_0\eta_j/\eta_0$. In figure 4a the sensitivity is plotted as a function of the thickness of the active layer. We used an amorphous silicon layer for the calculations assuming the wavelength of incoming light to be 550nm (green). For the calculations we took into account the complex refractive index ($n=\eta+i\kappa$) of amorphous silicon. The same parameters were used for the calculations of figure 4a, 4b and 4c. The sensitivity increases exponentially until nearly all light is absorbed (d_j=200nm-300nm) and the sensitivity remains constant. Besides the dc sensitivity, we are interested in the interaction of the standing wave with the semi transparent sensor. Therefore we calculated the differential sensitivity (DS) of the spectrometer corresponding to the interference term in equation 3.

$$\begin{aligned} DS(d_m, \lambda) &= -k_0 \exp(-\alpha_j d_j) \int_0^{d_j} \cos\left(\frac{4\pi}{\lambda}\left(\eta_j (d_j - x) + d_m\right)\right) dx \\ &= \frac{k_0 \lambda}{\pi \eta_j} \exp(-\alpha_j d_j) \cos\left(\frac{4\pi d_m}{\lambda} + \frac{2\pi \eta_j d_j}{\lambda}\right) \cdot \sin\left(\frac{2\pi \eta_j d_j}{\lambda}\right) \end{aligned} \tag{5}$$

The differential sensitivity of the active layer is given in figure 4b. We calculated the differential sensitivity (thin solid lines) for two positions of the mirror ($d_m=\lambda/4$ and $d_m=\lambda/2$) resulting in a phase shift of the standing wave of 90°. The bold solid lines in figure 4b correspond to the upper and lower limit of the differential sensitivity. For thin active layers we observe an increase of the differential sensitivity with increasing thickness of the active layer. In this case the layer thickness is a fraction of the wavelength ($d_j \ll \lambda/\eta_j$) and the increase of the differential sensitivity is caused by the increased absorption of the active layer. The differential sensitivity reaches its maxima for an active layer thickness of 30nm. For thicker active layers the differential sensitivity decreases again, because more and more light is observed in the active layer, so that for thicker active layers only a small amount of light is reflected at the mirror.

A further figure of merit is the standing wave effect (SWE). The standing wave effect is typically calculated for devices like solid-state lasers or resonant cavity detectors but can be applied for the standing wave spectrometer as well [11]. The standing wave effect defines the ratio between the average light absorbed in the complete active layer versus the average light absorbed in a period of the standing wave. The standing wave effect can be described by

$$SWE(d_m, \lambda) = \frac{\frac{1}{d_j} \int_0^{d_j} |E(x, d_m, \lambda)|^2 dx}{\frac{2\eta_j}{\lambda} \int_0^{\lambda/2n_j} |E(x, d_m, \lambda)|^2 dx} = \frac{\frac{1}{d_j} \int_0^{d_j} I_j(x, d_m, \lambda) dx}{\frac{2\eta_j}{\lambda} \int_0^{\lambda/2n_j} I_j(x, d_m, \lambda) dx} \tag{6}$$

Combing equation 3 and 6 results in equation 7.

$$SWE(d_m, \lambda) = \frac{\lambda}{2\eta_j d_j} \cdot \frac{1 - \exp(-2\alpha_j d_j) + \frac{\lambda \alpha_j}{\pi \eta_j} \exp(-\alpha_j d_j) \cdot \cos\left(\frac{4\pi d_m}{\lambda} + \frac{2\pi \eta_j d_j}{\lambda}\right) \cdot \sin\left(\frac{2\pi \eta_j d_j}{\lambda}\right)}{1 - \exp\left(-\frac{\alpha_j \lambda}{2\eta_j}\right) + \exp(-\alpha_j d_j)\left(\exp\left(\frac{\alpha_j \lambda}{2\eta_j}\right) - 1\right)} \tag{7}$$

Again we neglected the effect of the subsystems S_2 (τ_2=1) on the standing wave. Therefore, the standing wave effect depends on the material properties of the active layer, the wavelength of the incident light and the air gap between the sensor and the mirror. The standing wave effect as a function of the thickness of the active film is plotted in figure 4c. Again the modulation were determined for two mirror positions of $d_m=\lambda/4$ and $d_m=\lambda/2$ (thin solid lines). The bold solid lines correspond to the upper and lower limit of the SWE. For thin active layers most of the light is transmitted through the sensor and a strong modulation is detected. In this case the active layer is thinner than the period of the standing wave. Therefore, the SWE reaches its maxima. The maxima is reduced to SWE(d_j <<λ)=1.92 in comparison to the ideal standing wave spectrometer (SWE(d_j<<λ)=2) due to the absorption of the amorphous silicon layer. The standing wave effect is reduced to SWE=0.5-1 for active layer thicknesses of 30-200nm. With increasing thickness the modulation decreases, because the transmission of the sensor is reduced.

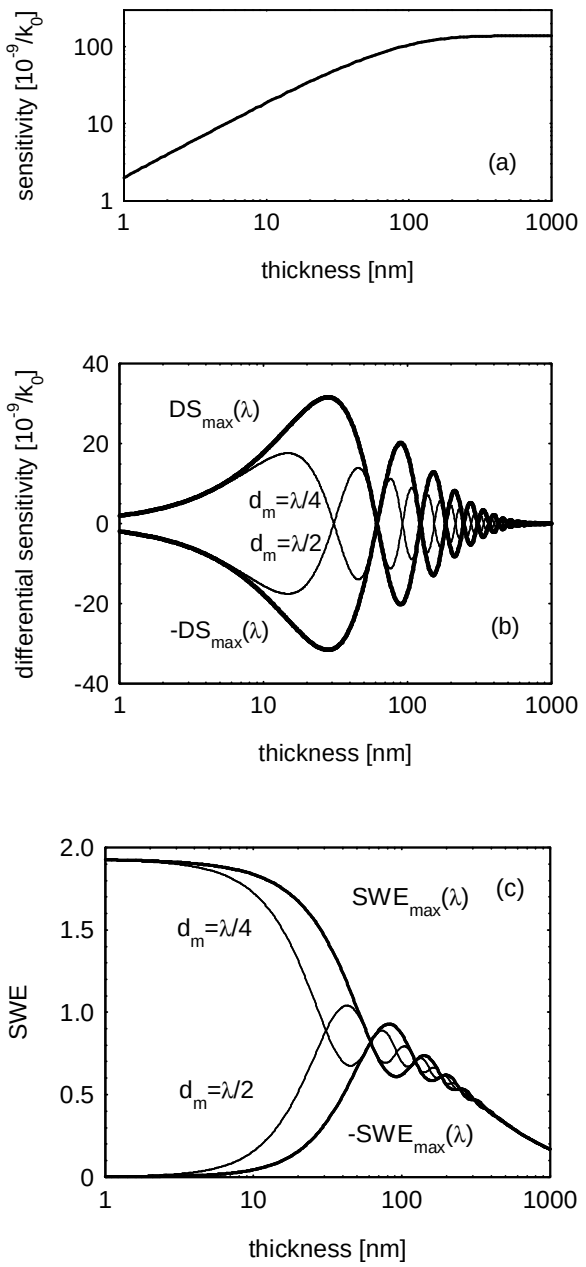

Fig. 4: Sensitivity (a), differential sensitivity (b) and Standing wave effect (SWE) (c) of a semi transparent detector as a function of the thickness of the active layer. Amorphous silicon was used for the calculations. Furthermore, we used a wavelength of 550nm (green) for the calculations. The semi transparent sensor is described only by the complex refractive index of amorphous silicon.

The calculations in figure 4a-4c clearly illustrate the relation between the dc sensitivity, the differential sensitivity and the active layer thickness and the position of the mirror. However, the deduction of an optimal active layer thickness from the calculations can only used as a rough estimation, because the sensor is only described by the active layer and the effect of the subsystems S_1, S_2 on the optical generation was neglected. However, further investigation shows that the effect of the multi-layer system on the optical generation profile should be low [13], so that the standing wave moves nearly unaffected through the sensor. The interaction of the standing wave with the semi transparent sensor for $d_j=k\cdot\lambda/4\eta_j$ (k=2,4,6,..) is the weakest, whereas the interaction between the standing wave and the senor is the strongest for $d_j= k\cdot\lambda/4\eta_j$ (k=1,3,5,..).

4. RESULTS

4.1 Simulation experiments

It has already been pointed out that the device design requires a trade-off between sensitivity and selectivity of the semi transparent sensor. But so far the optics of the Fourier spectrometer has been discussed taking into account an ideal absorber, which not disturbs the propagation of the standing wave. However, to benchmark the quality of the detector the optical properties of all individual layers of the optical detector, the reflection of the light at all interfaces (e.g. air/detector) and the phase conditions have to be considered.

The simplest device structure, which can be applied for sampling a standing wave, is a photoconductor using a coplanar contact configuration. An example for such a structure is given in figure 2a. The structure has the advantage that metal contacts can be used to apply an electric field to the film. We will again use amorphous silicon as the active material of the semi transparent sensor. Amorphous silicon can be prepared by plasma enhanced chemical deposition (PECVD) at low deposition temperature on neutral substrates like glass or plastic substrates.

Calculations of the reflection of the coplanar photoconductor for various thicknesses of the active layer on glass substrates indicate that such a structure has a high reflection even without a mirror [12]. Only for wavelengths of $\lambda=2d_j\cdot\eta_j$ the reflection of the detector is reduced due to destructive interference. d_j and η_j correspond to the thickness and the refractive index of the active layer. The reflection is reduced to a minimum of 4-5% caused by the reflection of light at the air/glass interface. For other wavelengths the reflection is increase up to more than 50% in the visible range (380nm-780nm) using amorphous silicon films of interest (d_j=30nm-60nm) [12].

In order to realize a sensor with a reduced reflection and a higher transmission we used simple multi-layer stacks based on a sandwich of two transparent conductive oxide (TCO) layers (e.g. ZnO, SnO_2, ITO), which act as a contact electrode and an amorphous silicon layer. The amorphous silicon layer (a-Si:H) is embedded between the two TCO-layers. Calculations indicate that the reflection of the multi-layer stack can be reduced over a wide range depending on the spectral range of interest and the thickness of the individual layers of the sandwich structure.

Hence, most of the light is transmitted through the sensor, so that the light can be reflected at the mirror. The layer stack behaves like a simple optical band pass [9]. By adapting the thickness of the individual layers of the stack, the sensor can be optimized for certain wavelengths. For shorter wavelengths the width (FWHM) of the transmitted spectrum is reduced because light is absorbed in the amorphous layer.

The resolution of the spectrometer can be improved by the separation of the optical generation from the extraction of photo-generated carriers. The regions of optical generation and extraction of carriers can be separated by using doped layers. Light is absorbed in the doped layers, but the photo-generated carriers do not contribute to the photocurrent. The photoconductor between the transparent electrodes can be substituted by a pin-diode. Therefore, only the carriers created in the intrinsic layer of the diode contribute to the over all photocurrent. The carriers in the p-and n-layer recombine due to the low lifetime in the doped regions.

Based on the different device designs (coplanar photoconductor, layer stacks TCO/photoconductor/TCO and TCO/pin-diode/TCO) we have calculated the optical generation for different positions of the mirror (fig. 6). In

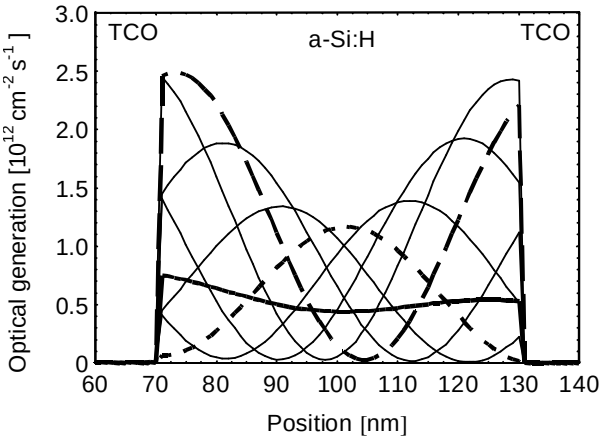

Fig. 6: Optical generation within the transmissive sensor based on glass/TCO/photo-conductor/TCO for different positions of the mirror. The optical generation has been calculated for the wavelength of 550nm. Bold line (no mirror), short dashed line ($d_{air}=\lambda/n_{air}$), long dashed line ($d_{air}=5/4\cdot\lambda/n_{air}$).

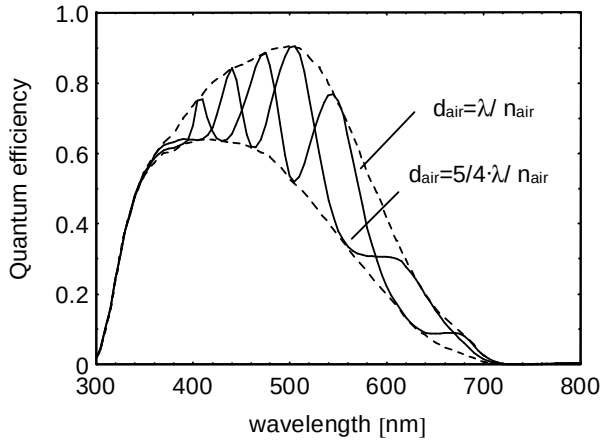

Fig. 7: Quantum efficiency of the transmissive sensor based on glass/TCO/photoconductor /TCO for different positions of the mirror. The optical generation has been calculated for the wavelength of 550nm (green). Bold line (no mirror), short dashed line ($d_{air}=\lambda/n_{air}$), long dashed line ($d_{air}=5/4\cdot\lambda/n_{air}$).

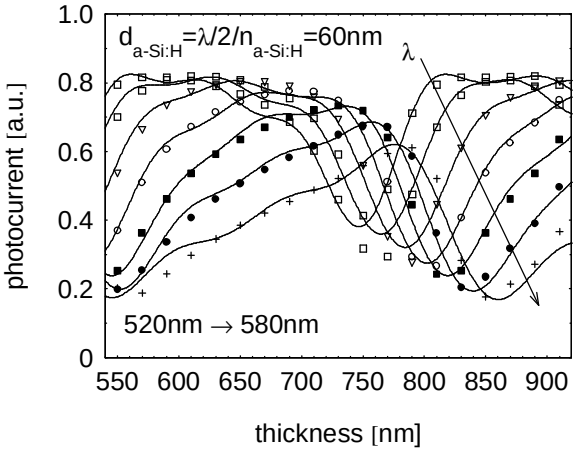

Fig. 8: Modulation of the photocurrent as a function of position of the mirror for a photoconductor on a glass substrate.

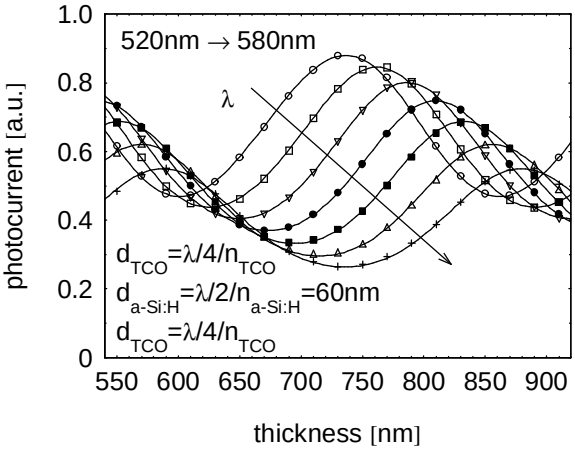

Fig. 9: Modulation of the photocurrent as a function of position of the mirror for a photoconductor on a glass substrate.

order to estimate the performance of a spectrometer in the visible range we have taken a 60nm thick photoconductor/diode corresponding to an optimized wavelength of 550nm (green light). The optical generation within a TCO/photoconductor/TCO structure is shown in figure 6. A pin-diode based on a layer sequence of $d_p=\lambda/8/n_{a\text{-}Si:H}$, $d_i=\lambda/4/n_{a\text{-}Si:H}$, $d_n=\lambda/8/n_{a\text{-}Si:H}$ was used. The optical generation clearly indicates that the standing wave moves through the sensor as the mirror changes its position. The bold line represents the optical generation without a mirror. The long dashed line based on a calculation of a layer structure with an air gap of $d_{air}=\lambda/n_{air}$, whereas the short dashed line corresponds to a shift of the mirror by 120nm, which is approximately a quarter of the wavelength or a shift of the standing wave by 90°. In figure 7 the corresponding quantum efficiency of the sensor is plotted for the two specified positions of the mirror. The dashed lines indicate the limit of the modulation of the quantum efficiency. The quantum efficiency for this specific wavelength changes between 0.36 and 0.75.

Based on the calculated sensitivity we have determined the transient modulation of the photocurrent for a constant velocity of the mirror. We observed a slight deviation of the transient photocurrent from an ideal sinus signal for

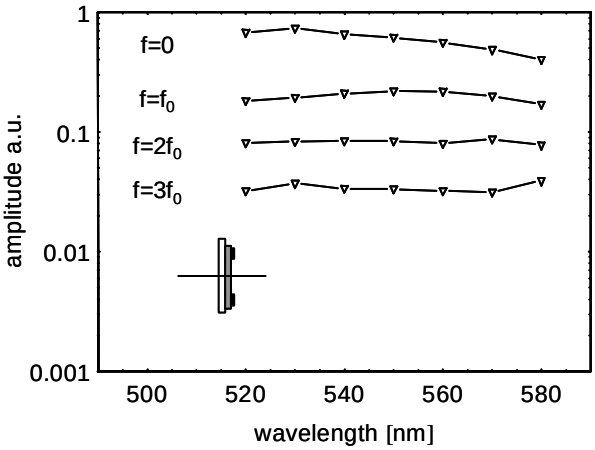

Fig. 10: Amplitude of the Fourier transformed photocurrent based on a coplanar photoconductor (∇).The parameters correspond to the values used in figure 8.

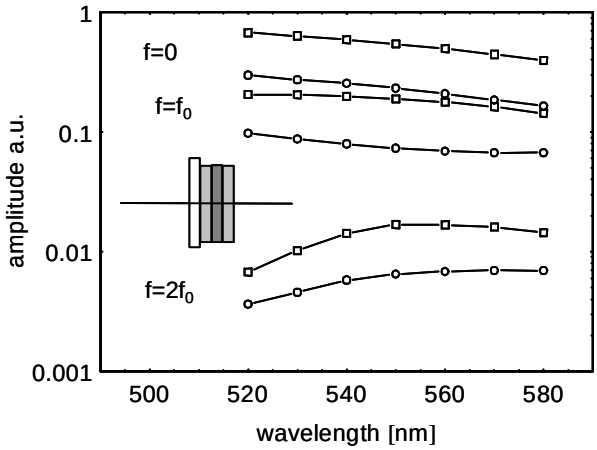

Fig. 11: Amplitude of the Fourier transformed photocurrent based on a TCO/photoconductor /TCO (□) and a TCO/pin-diode/TCO structure (O). The parameters correspond to the values used in figure 9.

the TCO/photoconductor/TCO and the TCO/pin-diode/TCO configuration, whereas the photocurrent of the coplanar structure exhibits a strong deviation from the ideals sinus function. The modulated photocurrent of the coplanar structure is given in figure 8 and 9. The position of the mirror was modulated by changing the gap between the detector and the mirror from d_m=540nm to d_m=920nm. The photocurrent for different wavelengths as a function of the gap between the detector and the mirror is plotted for a photoconductor with a thickness of 60nm. The wavelength ranges from 520nm to 580nm. As it can be seen the modulation of the photocurrent strongly deviates from the ideal case of a sinus/cosinus functions. The same calculations were performed for a sandwich structure with an active region of 60nm amorphous silicon. The 60nm correspond to a half wavelength layer. The TCO layers introduced on both sides of the active film have a thickness of a quarter wavelength. The position of the mirror was again modulated by 360nm from 540nm to 920nm. In this case the modulated photocurrent is distinctly closer to an ideal sinus/cosinus function.

Afterwards, we have transformed the signal from the time-domain into the frequency domain. In figure 10 and 11 the amplitudes of the Fourier transformation as a function of the wavelength are shown. The frequency f_0 represents the key-frequency ($f_0=v/\lambda_0$) and the amplitude f=0 corresponds to the dc photocurrent in the time domain. The calculations for the coplanar photoconductor showed strong contributions of the harmonic frequencies to the transient photocurrent. The side bands for the TCO/ photoconductor/TCO and the TCO/pin-diode/TCO structure are distinctly reduced corresponding to –20dB attenuation. The performance of the TCO/photoconductor/ TCO and the TCO/pin-diode/TCO structure are similar, but the sensitivity of the TCO/photoconductor/TCO structure is higher. In the case of the TCO/photoconductor/TCO structure a 60nm thick layer contributes to the photocurrent, whereas in for TCO/pin-diode/TCO structure only the 30nm thick absorption layer contributes to the photocurrent. Figure 11 clearly points out that structures with antireflection coating are clearly superior to simple structures, which are not adapted to the specific wavelength region.

4.2 Experimental Results

Based on the calculations of the last section it can be concluded that the optical properties of a sandwich structure are superior to a simple coplanar photoconductor structure without antireflection coatings. Therefore, we will focus in this section on experimental results of sandwich structures. The amorphous silicon detectors were deposited in a multi-chamber PECVD (plasma enhanced chemical vapor deposition) system at 210°C on glass substrates coated with flat TCO_I (transparent conductive oxide). We used a pin diode as a photo detector. P- and n-type doped layers were realized by adding trimethylboron and phosphine to the deposition gases silane and hydrogen, respectively [14]. The i-layers were prepared by using only silane and hydrogen. Afterwards the second TCO_{II} layer was prepared. The TCO layers were realized by rf-magnetron sputtered ZnO [13]. To prevent a damage of the amorphous layer system the TCO_{II} layer was prepared at room temperature. A more detailed description of the preparation conditions and the properties of the TCO-layer are described in reference 13. The multi-layer stacks on glass were patterned using photolithography and reactive ion etching. The detectors have an active area of 10 mm^2.

Three different samples will be compared in the following. The influence of the thickness of the doped and intrinsic layers on the device performance of the semi transparent sensor was investigated. All three samples were prepared with 155nm thick TCO_I- and TCO_{II}-layers. The TCO-layers corresponds to a half wavelength plate ($\lambda/2/n$) assuming a wavelength of 633nm. The device design was optimized for a wavelength of 633nm, so that the performance can be evaluated using a HeNe laser as a light source.

In the case of sample A the amorphous layer stack has a thickness of $\lambda/2/n$ with an active layer thickness (i-layer) of $\lambda/4/n$. Sample B is characterized by an amorphous layer stack of $3\cdot\lambda/4/n$ thickness. The active layer thickness is $\lambda/2/n$ and the doped n- and p-layer thickness is $\lambda/8/n$.

	TCO_I	**p-layer**	**i-layer**	**n-layer**	**TCO_{II}**
Sample A	155nm	19nm	39nm	19nm	155nm
Sample B	155nm	19nm	77nm	19nm	155nm
Sample C	155nm	39nm	77nm	39nm	155nm

Tab. 1: Parameters of the semi transparent sandwich structure on glass substrates.

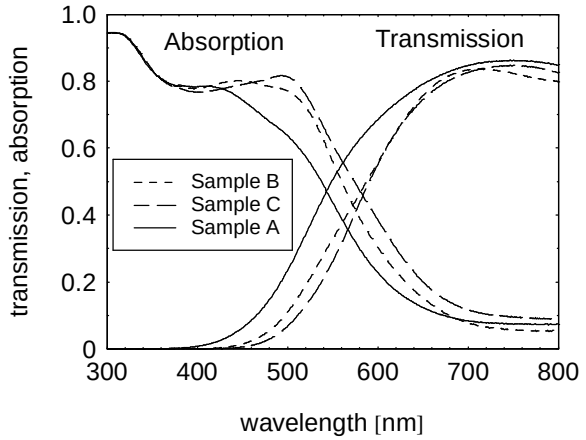

Fig. 12: Experimental measured transmission and absorption of the samples A, B and C (table 1).

Sample C based on a stack of λ/n with an active layer thickness (i-layer) of λ/2/n and a doped layer thickness of is λ/4/n.The absorption and the transmission of the three samples are shown in figure 12. The distinct increase of the transmission shifts to longer wavelength with increasing thickness of the layer stack.

For a wavelength of 633nm the transmission of sample A is 75%. The transmission of the sample B and C is 70%. Sample A, B and C exhibit an absorption for this particular wavelength of 15%, 20% and 25%, respectively. The absorption behavior is in opposite to the transmission (A=1-T-R) of the semi transparent sensor. The decrease of the absorption edge shifts to longer wavelength with increasing thickness of the layer stack of the pin-diode. The high absorption in the region between 300nm and 350nm is mainly caused by the absorption within the glass substrate and the TCO-layers.

The spectral response of the samples A, B and C measured from the front and the backside is shown in figure 13 and 14. The diodes were measured under short circuit conditions. The samples A and B are characterized by a p- and n-layer thickness of 19nm, whereas the p- and n-layer of the sample C is twice as thick. The thinner doped p- and n-layer of sample A and B leads to a higher spectral sensitivity for shorter wavelengths measured from the front (p-layer limitation) and the backside (n-layer limitation) of the sensor. Sample B and C are both characterized by an active intrinsic layer thickness of 77nm, whereas the i-layer of sample A is only 39nm thick. The difference in the design of the sensor is reflected in the red response. Due to the thicker absorption layer the spectral sensitivity of the samples B and C is enhanced for longer wavelengths. For a wavelength of 633nm the change of thickness leads to an enhancement of the spectral sensitivity by 50% up to more than 80 mA/W for sample B and C.

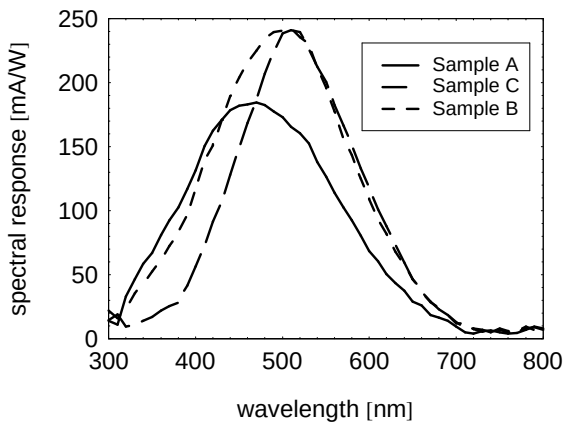

Fig. 13: Spectral response of the samples A, B and C were measured through the glass substrate (front side). The curves were measured under short circuit conditions.

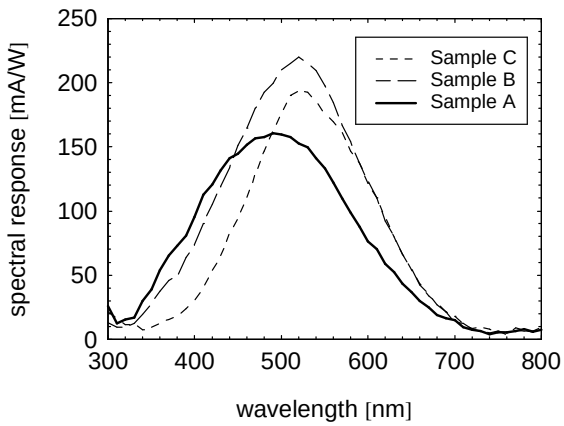

Fig. 14: Spectral response of the samples A, B and C were measured through the glass substrate (back side). The curves were measured under short circuit conditions.

In the next step the devices were characterized in combination with a tunable mirror. Details of the characterization will be described later.

5. DISCUSSION

The optical design of different semi transparent detectors has been discussed. The optical behavior of a sandwich structure is clearly superior to the behavior of a coplanar photoconductor structure without anti reflection coating. However, in addition to the optical aspects several other aspects have to be taken into account. A summary of the important device parameters is given in table 2. The processing of a coplanar structure is simpler than the fabrication of a sandwich structure. Metal contacts can be used to realize the electrodes of the coplanar detector. No transparent contacts are necessary to form the contacts. The sandwich structure however requires transparent contacts like ITO, ZnO or SnO_2. In this case it does not matter whether the semiconductor structure is realized as a photoconductor structure or a diode structure. In both cases the fabrication of a sandwich structure requires a better control of the process parameters. The processing of the ultra thin diode requires very smooth TCO layers. This is of particular interest for the TCO_I-layer. The TCO_I-layer should be as smooth as possible. After sputtering the TCO_I-layer the pin-diode is deposited. To avoid damage of the underlying amorphous layer the TCO_{II}-layer has to be sputtered very carefully. A more detailed description of the deposition conditions is given in reference 12.

In respect to the alignment of the sensor, the mirror and the incoming light beam the sandwich structure is beneficial, because the structure is less sensitive to sensor misalignment within the plane of the sensor. Therefore the sensor design is independent of the spot size of the incoming light beams. In the case of the coplanar structure the spot size has to be larger than the gap of the electrodes. Furthermore the spot has to be uniform. Otherwise the conductivity is limited by the position of the lowest illumination intensity. The situation can be improved by interdigitated contacts. On the other hand more light is reflected at the interdigiated metal contacts, so that an optimized design of the contacts is required.

Both detectors can be combined with active matrix addressing to realize 1D and 2D arrays. An active matrix addressing is advantages because it can be combined with pixel processing electronics. Advanced pixel electronics facilitates preprocessing of the sensor signal like data compression or filtering of the sensor signal. An example of an adaptive filter concept in combination with a standing wave spectrometer is given in reference 17.

The transient behavior of the sensor is another important parameter to characterize the spectrometer. The response time of the coplanar structure is limited by the majority carrier lifetime, the mobility, the applied electric field and the contact geometry. Photocurrent transient responses of the amorphous silicon in the range of µs can be reached. The geometric capacitance of the structure is very small, so that the RC constant of the sensor leads to no

	Coplanar Photoconductor structure	**Sandwich structure**
Current flow (standing wave)	perpendicular	Parallel
Processing	simple	complicated (several layers required, shunts between the two TCO-layers)
Contacts	Metal	Transparent
Light spot	Uniform (requires good alignment)	Independent
Read-out mode	Change of photoconductivity	Diode behaves like a current source
Read-out Electronic	High electric field required	High geometric capacitance requires special amplification circuits
Transient behavior	Determined by a the majority carrier mobility, lifetime, electric field and the contact geometry design	Limited by the geometric capacitance of the sandwich structure

Tab. 2: Comparison of the detector concepts

limitation of the transient behavior of a coplanar sensor structure. However the RC constant limits the transient response of the sandwich structure. The geometric capacitance of the sandwich structure is large, due to the vertical device structure. In addition the RC constant depends on the conductivity of the contacts, which are so far limited by the conductivity of the transparent conductive oxide layers. First experimental results exhibit transient responses of the sandwich structure in the range of 10-100μs [16].

6. SUMMARY

The optical design of a novel spectrometer based on sampling a standing wave has been presented. The spectrometer consists of a partially transmissive sensor and a tunable mirror. A simple analytical model has been developed to evaluate different device designs of the partially transmissive sensor. The calculations determine the upper limit of the performance of such a device. The performance of the Fourier spectrometer can be distinctly improved by an adapted device design including anti reflection coatings. The presented novel Fourier spectrometer reduces the number of components to a minimum, simplifies the setup to a linear arrangement of a detector and a mirror and facilitates the realization of 1 or 2D spectrometer arrays.

ACKNOWLEDGEMENT

The authors like to thank W. Beyer, E. Bunte (Research Center Jülich), P. Herzog, B. Hill (University of Technology Aachen), Michel Rosa (Palo Alto Research Center) for many helpful discussions, H.Büchner, G. Jäger (Technical University Ilmenau) for interesting new ideas and the group of F. Finger and B. Rech (Research Center Jülich) for technical support.

REFERENCES

[1] P.M. Zavracky, K.L. Denis, H.K. Xie, T. Wester, P. Kelley, SPIE Proc. 3514, p. 179 (1998).
[2] Manzardo, O.; Guldimann, B.; Marxer, C.R.; de Rooij, K.F.; Herzig, H.P., IEEE/LEOS International Conference on Optical MEMS (2000)
[3] Manzardo, O.; Herzig, H.P.; Marxer, C.R.; de Rooij, N.F. SPIE Proc. 3878 p. 39 (1999).
[4] Patrick G. Herzog, Virtual Fabrics or Multispectral Imaging in B2B, The First European Conference on Color in Graphics, Imaging and Vision (CGIV), France (2002).
[5] D.A.B. Miller, IEEE J.of Quantum Electronics, Vol. 30 No. 3, 732 (1994).
[6] H.-J. Buechner, German Patent: DE 33 00 369 (1983),
G. Jaeger, H.-J. Buechner, German Patent: DE 36 12 1221 (1986),
A. Haiduk, A. Kottwitz, R. Legler, H.-J. Buechner, K. Gerhardt, German Patent: DE 40 17 201 (1990).
[7] D.H. Alexander, K. Ishizuka, R.N. Sato, United State Patent 4,443,107 (1984).
[8] H.L. Kung, S.R. Bhalotra, J.D. Mansell, D.A.B. Miller, 2000 IEEE/LEOS International Conference on Optical MEMS;
H.L. Kung, S.R. Bhalotra, J.D. Mansell, D.A.B. Miller, J.S. Harris Jr., IEEE Selected Topics in Quantum Electronics, 8, 98 (2002).
S.R. Bhalotra, H.L. Kung, J. Fu, N.C. Helman, O. Levi, D.A.B. Miller, J.S. Harris, Jr., 2002 IEEE/LEOS International Conference on Optical MEMS;
[9] Z. Knittl, Optics of Thin Films (Wiley, London 1976)
[10] H. Stiebig, A. Kreisel, K. Winz, M. Meer, N. Schultz, Th. Eickhoff, H. Wagner, Proc. First World Conference on Photovoltaic Energy Conversion (WCPEC), 603 (1994).
[11] D. Knipp, P.G. Herzog, H. Stiebig, IEEE Transactions on Electron Devices, Vol. **49**, pp. 170-176 (2002).
[12] M.S. Ünlü, S. Strite, J. Appl. Phys. **78** (2), 607 (1995).
[13] D. Knipp, M. Rosa, H. Stiebig, H.-J. Büchner, R.A. Street, Mat. Res. Soc. Proc. Vol. 687 (2001) in print.
[14] O. Kluth, A. Löffl. S. Wieder, C. Beneking, L. Houben, B. Rech, H. Wagner, S. Waser, J.A. Selvan, H. Keppner, Proc. 26th IEEE PVSEC, pp. 715-718 (1997).
[15] W. Luft, Y. Tuso, Hydrogenated amorphous silicon alloy deposition processes, Marcel Dekker, Inc., 1993.
[16] H. Stiebig, H.-J. Büchner, E. Bunte, V. Mandryka, D. Knipp, G. Jäger, Thin Solid Films (2002) in print.
[17] Sameer R. Bhalotra, Helen L. Kung, Yang Jiao, David A. B. Miller, Optics Lett. **27**, 1147-1149 (2002).